Electronic structure and hybridization effects in Hume-Rothery alloys containing transition elements

G. Trambly de Laissardière, D. Nguyen Manh,* L. Magaud, J. P. Julien, F. Cyrot-Lackmann, and D. Mayou
Laboratoire d'Etudes des Propriétés Electroniques des Solides, CNRS, Boîte Postale 166, 38042 Grenoble Cedex 9, France
(Received 5 April 1995)

We present a systematic study of the electronic structure of Al-based Hume-Rothery alloys containing transition elements performed with the use of the linear muffin-tin orbital in atomic-sphere approximation method. Our analysis focuses on the formation of the pseudogap at the Fermi level leading to the stability of materials containing transition-metal elements in small concentration. From the self-consistent calculated density of states, we observe a strong deviation from the two classical limits: (a) the Friedel-Anderson virtual bond state's model and (b) the nearly-free-electron diffraction by some Bragg planes in the usual Hume-Rothery picture of simple metal alloys. Transition-metal atoms have a crucial role on electronic structure via the combined effect of the *sp-d* hybridization and of a strong interaction between the Fermi surface and a predominant Brillouin zone.

I. INTRODUCTION

A. Hume-Rothery alloys

The so-called Hume-Rothery phases[1] are metallic alloys or compounds for which the average number of valence electrons per atom is crucial in determining the total energy, whereas the size and the electronegativity factors are not very important. They are characterized by the presence of strong diffraction peaks related to strong scattering of electrons by peculiar Bragg planes. In such system, the Hume-Rothery rule[1] correlates the crystalline structure and the average number of electrons per atom. Many of these phases are *s* or *sp* elements only. In these cases, Jones[2] pointed out that the structure of Hume-Rothery alloys is stabilized when the number of conduction electrons per atom is such that the Fermi sphere touches a "*predominant Brillouin zone,*" constructed by the Bragg planes located in the vicinity of the Fermi sphere. In such a case,

$$2k_F \approx K_i \ , \tag{1}$$

where k_F is the momentum of electrons at Fermi energy (E_F) and K_i the reciprocal vectors corresponding to the Bragg planes of the predominant Brillouin zone. The pure noble metals and the pure II to IV elements obey well these rules.[1–3] The *sp* density of state (DOS) of Hume-Rothery alloys is now well described by the model of nearly free electrons. The diffraction by Bragg planes leads to the formation of a pseudogap located near E_F [Eq. (1)].

Recently, Hume-Rothery–alloy behavior has been found in aluminum-based quasicrystals. In particular, the role of the diffraction by Bragg planes has been studied by Friedel and Denoyer[4] for the AlLiCu *i* quasicrystals (*i* denotes icosahedral), by Smith and Ashcroft[5] for a hypothetical aluminum quasicrystalline phase, and by Vaks, Kamyshenko, and Samolyuk[6] for quasicrystal alloys of simple noble metals. From *ab initio* calculation, the concept of a universal pseudogap has also been shown by Fujiwara[7,8] for approximants of quasicrystals. Finally, specific-heat[9] and spectroscopy[10] measurements show a large reduction of the DOS at the Fermi level as compared to the free-electron value.

In this paper, we do not discuss the general transport properties of Hume-Rothery alloys in detail, but it should be mentioned that quasicrystalline phases have abnormal behavior compared to crystalline Hume-Rothery phases with the same constituents. For reviews on transport properties in crystalline and quasicrystalline Hume-Rothery phases see, for instance, Refs. 3 and 11 and Refs. 12 and 13, respectively.

B. Transition metals in Hume-Rothery alloys

Many crystalline (Al_6Mn,[14] Al_7Cu_2Fe,[15] Al_9Co_2,[16,17] Al_5Co_2,[17] Al_3Ni,[16] etc.) and quasicrystalline (*i*-AlCuFe,[18] *i*-AlCuPd,[19] *i*-AlPdMn,[20] *i*-AlPdRe,[21] etc.) Hume-Rothery phases contain transition-metal (TM) atoms.

In the case of quasicrystalline phases, the influence of TM on electronic structure and stability is well established experimentally,[22,23] but not clearly understood. An interesting result is the strong correlation between the minimum of conductivity and the change of sign in the Hall effect with the concentration of Fe in *i*-AlCuFe.[23]

The presence of TM elements complicates the analysis of the electronic structure in terms of nearly free electrons. In his original description of Hume-Rothery alloys containing transition elements, Raynor[24] assumed the mechanism of charge transfer from the conduction band (*sp* band) into the *d* band to compensate the unpaired spins of the TM elements, and then, the TM was accordingly assigned to a negative valence. This theory has been applied to the study of the electronic stabilization of many crystalline alloys such as Al_6Mn,[14] Al_7Cu_2Fe,[15] Al_9Co_2,[16,17] Al_5Co_2,[17] and Al_3Ni (Ref. 16) compounds, and recently Al-based quasicrystals.[18] Experimentally, the valence of TM cannot be estimated very accurately

but[18,24] it generally lies between -1 and -3 electrons per TM atom. Nevertheless, this mechanism assumes an important charge transfer on TM atoms, which seems to be unrealistic given the small difference of electronegativity and radii between different constituents. Indeed, experimental results[25] on Al-TM alloys with low TM concentration (typically less than 30%) show a charge transfer from the conduction *sp* states to the *d* states on TM atoms that is less than 0.5 electron per TM atom. This seems to be in contradiction with the strong charge transfer proposed by Raynor.

Theoretically, several studies of the electronic structure of transition-metal elements have been performed. Friedel[26] first analyzed the importance of TM on the electronic stability of *sp* alloys containing a small concentration of TM atoms. He considered the impurity limit and proposed a model containing one discrete *d* state of TM dissolved in a free *sp*-electron matrix. The hybridization between this *d* state and free states forms the so-called virtual bound state. In this model,[26,27] which does not take into account the diffraction by Bragg planes, the *d* band is a Lorentzian and the conduction band (*sp* states) is not modified by the presence of the *d* state (compensation theorem). Recently, Friedel[28] also discussed the influence of diffraction by Bragg plane on the electronic structure of TM elements in quasicrystals. Moreover, the influence of band structure of Al on 3*d* impurity has been studied by a self-consistent calculation using the Korringa-Kohn-Rostoker Green-function method,[29] and recently by a self-consistent Green-function linear-muffin-tin-orbital method.[30] These calculations show a significant deviation of the *d* band from the Lorentzian virtual bound state due to the combined effect of the *sp*-electron scattering by the Al pseudopotential and the *sp-d* hybridization.

In the case of the Al_2Ru semiconductor, we predicted[31] from *ab initio* calculation the formation of gap due to *sp-d* hybridization, which has been confirmed experimentally.[32] We also proposed a simple model[33,34] to simulate the effect of *sp*-electron diffraction by a pseudopotential on *d* states in Hume-Rothery alloys containing TM atoms. This model confirms the strong deviation of the *d* band from the virtual bound state Lorentzian, and shows the formation of a pseudogap near the Fermi level in the *d* band. Moreover, the strong potential of *d* states increases the effect of diffraction by Bragg planes on conduction states (*sp* states). So the Hume-Rothery pseudogap in the conduction band is increased by *d* impurities via *sp-d* hybridization. On the other hand, the effect of the pseudopotential of a collection of discrete *d* states on a free-electron conduction band had been studied[35] and shows the possible formation of gaps (or pseudogaps) on the total DOS due to the pseudopotential of *d* states. These two approaches do not contradict each other but are complementary as they consider two limiting cases; these are the *d* impurity and the collection of *d* discrete states, respectively. In both cases, the combined effect of electron scattering by a pseudopotential and *sp-d* hybridization has a crucial effect on the electronic structure and electronic stabilization.

Recently, a large number of papers[36,37,38] have been devoted to the study of the role of transition-metal elements in real quasicrystals. All of them emphasize the importance of electron diffraction by a pseudopotential in the presence of strong *sp-d* hybridization. But the electronic structure of TM in real systems and its influence on the DOS and transport are not yet clearly understood.

The aim of this paper is to study systematically the self-consistent electronic structure of a series of real Hume-Rothery crystals containing a small concentration of TM atoms embedded in an aluminum matrix. Thirteen real crystals (Table I) have been studied. Their atomic structures are very different, and so we expect to determine general characteristics of Hume-Rothery alloys containing a small concentration of TM atoms embedded in Al. Some of these compounds have been investigated elsewhere: in Ref. 41, the stability of the Al_{12} TM structure has been studied, and in Ref. 42, the Al_3V and Al_3Ti DOS have been calculated. Our work confirms the presence of a pseudogap near the Fermi level, and the crucial role of the transition-metal element on the increase of this pseudogap and the stability of these structures.

In Sec. II, we describe the *ab initio* method and studied alloys. The results of the calculated DOS in these compounds are presented in Sec. III. In Sec. IV, we focus on the combined effect of pseudopotential scattering and *sp-d* hybridization. Conclusions are given in Sec. V.

II. LMTO METHOD AND ITS APPLICATION TO STUDIED ALLOYS

The linear muffin-tin orbital (LMTO) formalism is well known and well described elsewhere.[43,44] However, we here review some results, which are useful for the purpose of this paper, concerning the construction of the basis set of orbitals $|\chi_{RL}\rangle$ and the physical rule of the structure constant in the Hamiltonian. The real space is divided in atomic spheres where the potential has a spherical symmetry, and in interstitial regions where the potential is flat. Using the atomic-sphere approximation (ASA), the sphere radii are chosen so that the total volume of the spheres equals that of the solid. In the interstitial region the kinetic energy is set to zero. Within these approximations, one builds a set of orthogonal orbitals $|\chi_{RL}\rangle$. $|\chi_{RL}\rangle$ is in fact calculated for a given energy $E_{\nu RL}$, usually taken at the center of gravity of the occupied part of the band, and $|\chi_{RL}\rangle$ is linearized from $E_{\nu RL}$ for other energy. $|\chi_{RL}\rangle$ is centered on the atomic site R and the greatest contribution of $|\chi_{RL}\rangle$ is inside the atomic sphere centered at R with the angular momentum L ($L=l,m$). In this basis set, the LMTO Hamiltonian can be written as

$$H_{RL,R'L'}=C_{RL}\delta_{RL,R',L'}+\Delta_{RL}^{1/2}S_{RL,R'L'}\Delta_{R'L'}^{1/2}, \quad (2)$$

where terms of order $(E-E_{\nu RL})^3$ and higher are neglected in the orthogonal representation. C_{RL} and Δ_{RL} are the potential parameters. The structure constant $S_{RL,R'L'}$ is the matrix element that couples the RL states and the $R'L'$ ones. When $S_{RL,R'L'}(L\neq L')$ equals zero we get bands having pure L. This has been done in the standard

TABLE I. Structure data of the studied alloys.

	Phase [Reference]	System	Structure space group	Atoms per unit cell	Lattice parameters (Å)	Atomic positions	x	y	z
a	Al_3Ti	Tetragonal	$D0_{22}$	4	$a=3.84$	Ti 2(a)			
	[Ref. 39 p. 1023]		$I4/mmm$		$c/a=2.234$	Al_1 2(b)			
						Al_2 4(d)			
b	$Al_{10}V$	Cubic	$Fd\bar{3}m$	44	$a=14.492$	V 16(c)			
						Al_1 16(d)	500	500	500
	[Ref. 39 p. 1030]					Al_2 48(f)	996	125	125
						Al_3 96(g)	055	055	026
						Vacancy 8(b)			
c	Al_3V	Tetragonal	$D0_{22}$	4	$a=3.722$	V 2(a)			
	[Ref. 39 p. 1029]		$I4/mmm$		$c/a=2.202$	Al_1 2(b)			
						Al_2 4(d)			
d	$Al_{12}Cr$[a]	Cubic	$Al_{12}W$	13	$a=7.507$	Cr 2(a)			
			Im3			Al 24(g)		184	309
e	$Al_{12}Mo$	Cubic	$Al_{12}W$	13	$a=7.5773$	Mo 2(a)			
	[Ref. 39 p. 926]		Im3			Al 24(g)		185	308
f	$Al_{12}Mn$[a]	Cubic	$Al_{12}W$	13	$a=7.47$	Mn 2(a)			
			Im3			Al 24(g)		184	309
g	Al_6Mn	Orthorhombic	$D2_h$	14	$a=7.5518$	Mn 4(c)		457	
			$Cmcm$		$b/a=0.8604$	Al_1 8(e)	324		
	[Ref. 39 p. 912]				$c/a=1.1746$	Al_2 8(g)	317	284	
						Al_3 8(f)		140	898
h	Al_7Cu_2Fe	Tetragonal	$P4/mnc$	40	$a=6.336$	Fe 4(e)		299	
					$c/a=2.347$	Cu 8(h)	278	088	
	[Ref. 39 p. 759]					Al_1 4(e)			134
						Al_2 8(g)	165		
						Al_3 16(i)	198	420	100
i	$Al_8Mg_3Si_6Fe$	Hexagonal	$P\bar{6}2m$	18	$a=6.62$	Fe 1(a)			
					$c/a=1.20$	Mg 3(g)	444		
	[Ref. 39 p. 823]					Si 6(i)	750		222
						Al_1 1(b)			
						Al_2 3(f)	403		
						Al_3 4(h)			231
j	Al_9Co_2	Monoclinic	$P2_1/c$	22	$a=6.2130$	Co 4(e)	264	615	333
					$b/a=1.0124$	Al_1 2(a)			
	[Ref. 40 p. 109]				$c/a=1.3772$	Al_2 4(e)	404	962	268
					$\beta=94.760°$	Al_3 4(e)	089	290	231
						Al_4 4(e)	389	193	999
						Al_5 4(e)	216	615	042
k	Al_5Co_2	Hexagonal	$D8_{11}$	28	$a=7.656$	Co 2(d)			
					$c/a=0.9918$	Co 6(h)	127		
	[Ref. 39 p. 717]		$P6_3/mmc$			Al_1 2(a)			
						Al_2 6(h)	470		
						Al_3 12(k)	194		942
l	Al_3Ni	Orthorhombic	$D0_{22}$	16	$a=6.5982$	Ni 4(c)	869		945
	[Ref. 39 p. 949]				$b/a=1.1142$	Al_1 4(c)	011		415
			$Pnma$		$c/a=0.7278$	Al_2 8(d)	174	053	856
m	Al_2Cu	Tetragonal	$C16$	6	$a=6.066$	Cu 4(a)			
	[Ref. 40 p. 111]		$I4/mcm$		$c/a=0.8035$	Al 8(h)	160		

[a]The real structure is $Al_{12}(Mn,Cr)$ (Ref. 40, p. 111). According to Ref. 39 (p. 913) $Al_{12}Mn$ exists in this structure but the exact atomic position is not known.

representation[44] and the resulting bands are the so-called "canonical bands." The influence of *sp-d* hybridization is discussed in Sec. IV, by setting the corresponding structure factor $S_{RL,R'L'}$ equal to zero.

Our aim is to analyze the role of transition metals (Ti, V, Cr, Mo, Mn, Fe, Co, Ni) on the electronic structure of Hume-Rothery alloys. Calculations are carried out on a series of crystals: Al_3Ti, $Al_{10}V$, Al_3V, $Al_{12}Cr$, $Al_{12}Mo$, $Al_{12}Mn$, Al_6Mn, Al_7Cu_2Fe, $Al_8Mg_3Si_6Fe$, Al_9Co_2, Al_5Co_2, Al_3Ni, and Al_2Cu. These alloys and their structures are reported in Table I. In each system, all TM atoms are equivalent except for Al_5Co_2 where they are al-

TABLE II. LMTO parameters used during self-consistent calculations: Number of **k** points in the first Brillouin zone (for $Al_{10}V$ the number of **k** points is increased from 729 to 17 576 during the paramagnetic self-consistent calculation), and muffin-tin-atomic sphere radii.

	Phase	Nb of **k** points	LMTO parameters muffin-tin sphere radii (Å)
	$Al_{(fcc)}$	1728	$R_{Al}=1.57$
a	Al_3Ti	1728	$R_{Al}=1.55, R_{Ti}=1.59$
b	$Al_{10}V$	729	$R_{Al_1}=1.77, R_{Al_2}=1.53,$
		17 576*	$R_{Al_3}=1.60, R_V=1.45$
c	Al_3V	1728	$R_{Al}=1.57, R_V=1.50$
d	$Al_{12}Cr$	1000	$R_{Al}=1.58, R_{Cr}=1.46$
e	$Al_{12}Mo$	1000	$R_{Al}=R_{Mo}=1.59$
f	$Al_{12}Mn$	1000	$R_{Al}=1.57, R_{Mn}=1.50$
g	Al_6Mn	552	$R_{Al}=1.57, R_{Mn}=1.41$
h	Al_7Cu_2Fe	384	$R_{Al}=1.55, R_{Cu}=1.48, R_{Fe}=1.39$
i	$Al_8Mg_3Si_6Fe$	1728	$R_{Al}=1.58, R_{Mg}=1.77,$ $R_{Si}=1.52, R_{Fe}=1.38$
j	Al_9Co_2	512	$R_{Al}=1.56, R_{Co}=1.41$
k	Al_5Co_2	1000	$R_{Al}=1.52, R_{Co}=1.40$
l	Al_3Ni	512	$R_{Al}=1.55, R_{Ni}=1.40$
m	Al_2Cu	1000	$R_{Al}=1.58, R_{Cu}=1.42$

most equivalent. Due to the small concentration of TM atoms, there are no nearest-neighbor pairs of TM atoms. In most of these alloys, the transition atoms are located in a highly symmetric environment. For instance, TM atoms are located in an icosahedral environment of Al atoms in $Al_{12}TM$ and in a nearly icosahedral environment of Al atoms in $Al_{10}V$.[45] This leads to a small crystalline field effect on the DOS and a large degeneracy of the five *d* orbitals of each TM atom.

The electronic structures are carried out using a scalar relativistic LMTO ASA code. The density functional formalism has been used within the local density approximation (LDA) with the von Barth and Hedin exchange and correlation potential.[46] This code includes combined corrections that correct errors from overlapping of the spheres and interstitial regions in the ASA. The basis functions include all angular moments up to $l=2$ and the valence states as follows: Al ($3s,3p,3d$), Cu ($4s,4p,3d$), Si ($3s,3p,3d$), Mg ($3s,3p,3d$), Mo ($5s,5p,4d$), and other TM ($4s,4p,3d$). Self-consistent calculations have been carried out in polarized spins case and in paramagnetic case. They are stopped when the total energy per atom is changed by less than 10^{-4} eV/atom per iteration. The **k** integration is performed using the tetrahedron method.[47] During the self-consistent calculation the number of **k** points in the reduced Brillouin zone has to be large enough. Then, for each system we have chosen a number of **k** points (Table II) such that if we double this number the DOS does not change significantly. In the frame of ASA, the sphere radii are chosen (Table II) to get a good compromise between the sphere overlaps (which has to be smaller than 30–35%) and the charge transfer between spheres (which is smaller than 0.3 electron per atomic sphere). Let us note that in these systems the total density of states does not change significantly if we change the radii by 10% even if the overlap becomes large (40–45%).

III. RESULTS

We have performed spin-polarized self-consistent calculations and found that all studied alloys are nonmagnetic. This is consistent with experimental results obtained by Dunlop, Gruner, and Caplin,[11] and *ab initio* calculations performed for Fe impurity in Al.[48] In the following we present LMTO's calculations in the paramagnetic case (without polarized spins).

A. Ground-state properties

The calculated equilibrium cohesive properties are given in Table III. Experimental results are also reported for comparison. Theoretical lattice constants are in good agreement with experimental data.

To compute the energy of formation, we subtract from the calculated LMTO total energy the sum of the calculated energies of each metallic constituent (Al, Cu, TM) with the proper multiplicity. The agreement with experimental measurements is fairly good for Al_3Ti, Al_3V, and $Al_{12}Mo$; for other alloys the difference between calculated and experimental values is larger. Nevertheless we should emphasize that the accuracy of calculated energy of formation within the muffin-tin approximation is not good as it imposes a spherical potential in each atomic sphere.

To our knowledge, very few cases of experimental determination of bulk modulus have been done on the studied alloys.

B. The electronic density of states

The position of the Fermi level E_F, calculated from the bottom of the Al *s* band, and DOS's at E_F are given in

TABLE III. Calculated (present work) and experimental cohesive parameters (at 298 K). $\Delta a = (a_{\text{calculated}} - a_{\text{experimental}}/a_{\text{experimental}})$, where $a_{\text{experimental}}$ is given in Table I.

		Lattice parameter		Bulk modulus (GPa)		Formation energy (eV/atom)	
	Phase	$a_{\text{calculated}}$ (Å)	Δa (%)	Calculated	Measured	Calculated	Measured
	$Al_{(fcc)}$	3.987	−1.5	86[a]	75.2[c]		
a	Al_3Ti	3.797[b]	−1.1	113[b]	105.6[d]	−0.35[b]	−0.38[e]
b	$Al_{10}V$	14.240	−1.7	96		−0.12	
c	Al_3V	3.723	−1.3	139		−0.30	−0.29[e]
d	$Al_{12}Cr$	7.393	−1.5	105		−0.06	
e	$Al_{12}Mo$	7.474	−1.4	109		−0.13	−0.16[e]
f	Al_2Mn	7.357	−1.5	107		−0.11	
g	Al_6Mn	7.408	−1.9	121		−0.24	−0.16[f]
h	Al_7Cu_2Fe	6.185	−2.4	132		−0.37	
i	$Al_8Mg_3Si_6Fe$	6.507	−1.7	94		−0.26	
j	Al_9Co_2	6.089	−2.0	108		−0.46	−0.31[e]
k	Al_5Co_2	7.524	−1.7	153		−0.69	−0.43[e]
l	Al_3Ni	6.481	−1.8	132		−0.56	−0.39[e]
m	Al_2Cu	5.915	−2.5	124	105[g]	−0.28	

[a]Calculated previously in Ref. 43: bulk modulus, 89.8 GPa.
[b]Calculated previously in Ref. 42: $a_{\text{calculated}} = 3.811$ Å, bulk modulus, 110 GPa, formation energy, 0.42 eV/atom.
[c]From Ref. 49.
[d]From Ref. 50.
[e]From Ref. 51.
[f]At 600 K, from Ref. 51.
[g]From Ref. 52.

Table IV. Total DOS (actually the sum of *s* Al, *p* Al, *d* Al, *s* TM, *p* TM, *d* TM, *s* Cu, *p* Cu, and *d* Cu self-consistent bands) of each studied alloy (except Al_2Cu) are presented in Fig. 1. The following general observations can be made from these figures.

(i) At low energy, the parabola due to the Al nearly-free-electron states is clearly seen. The peak of *d* states of TM is observed in the middle of the *sp* band. In the case of Al_7Cu_2Fe, the *d* peak of Cu is strong and located at an energy lower than that of the *d* peak of TM.

(ii) The Fermi level is found near a well-defined valley that splits the band between bonding and antibonding states. This valley, called the pseudogap, is due to diffraction of *sp* electrons by the Bragg planes corresponding to intense peaks in the diffraction pattern (Sec. IV A). The width of this pseudogap varies from ~0.3 to ~1 eV. Moreover this pseudogap is less pronounced in Al_3Ni, where the *d* peak is rather far from E_F. The total

TABLE IV. LMTO results. E_F: Fermi level calculated from the bottom of the 3*s* Al band; $n(E_F)$: total density of states (total DOS) at E_F; $n_{\text{TM}}(E_F)$: local DOS at E_F on TM atomic spheres (TM = Ti, V, Cr, Mo, Mn, Fe, Co, or Ni); $n_{\text{Al}}(E_F)$: local DOS at E_F on Al atomic spheres.

			LMTO results			
			$n(E_F)$	$n_{\text{TM}}(E_F)$		$n_{\text{Al}}(E_F)$	
	Phases	E_F (eV)	(states/eV atom)	(states/eV TM atom)	[% of $n(E_F)$]	(states/eV Al atom)	[% of $n(E_F)$]
	$Al_{(fcc)}$	12.1	0.30			0.30	100
a	Al_3Ti	10.3	0.40	1.02	64	0.19	36
b	$Al_{10}V$	11.0	~0.5	~1.6	~30	~0.4	~70
c	Al_3V	10.9	0.13	0.44	84	0.03	16
d	$Al_{12}Cr$	10.9	0.31	0.89	22	0.26	78
e	$Al_{12}Mo$	10.7	0.25	0.55	17	0.22	83
f	$Al_{12}Mn$	11.1	0.24	0.87	28	0.19	72
g	Al_6Mn	10.9	0.31	1.04	48	0.19	52
h	Al_7Cu_2Fe	10.9	0.29	0.72	25	0.24	58
i	$Al_8Mg_3Si_6Fe$	12.1	0.28	1.31	26	0.32	51
j	Al_9Co_2	11.0	0.25	0.41	30	0.21	70
k	Al_5Co_2	11.2	0.13	0.29	63	0.07	37
l	Al_3Ni	11.1	0.28	0.28	25	0.28	75
m	Al_2Cu	11.1	0.35			0.36	68

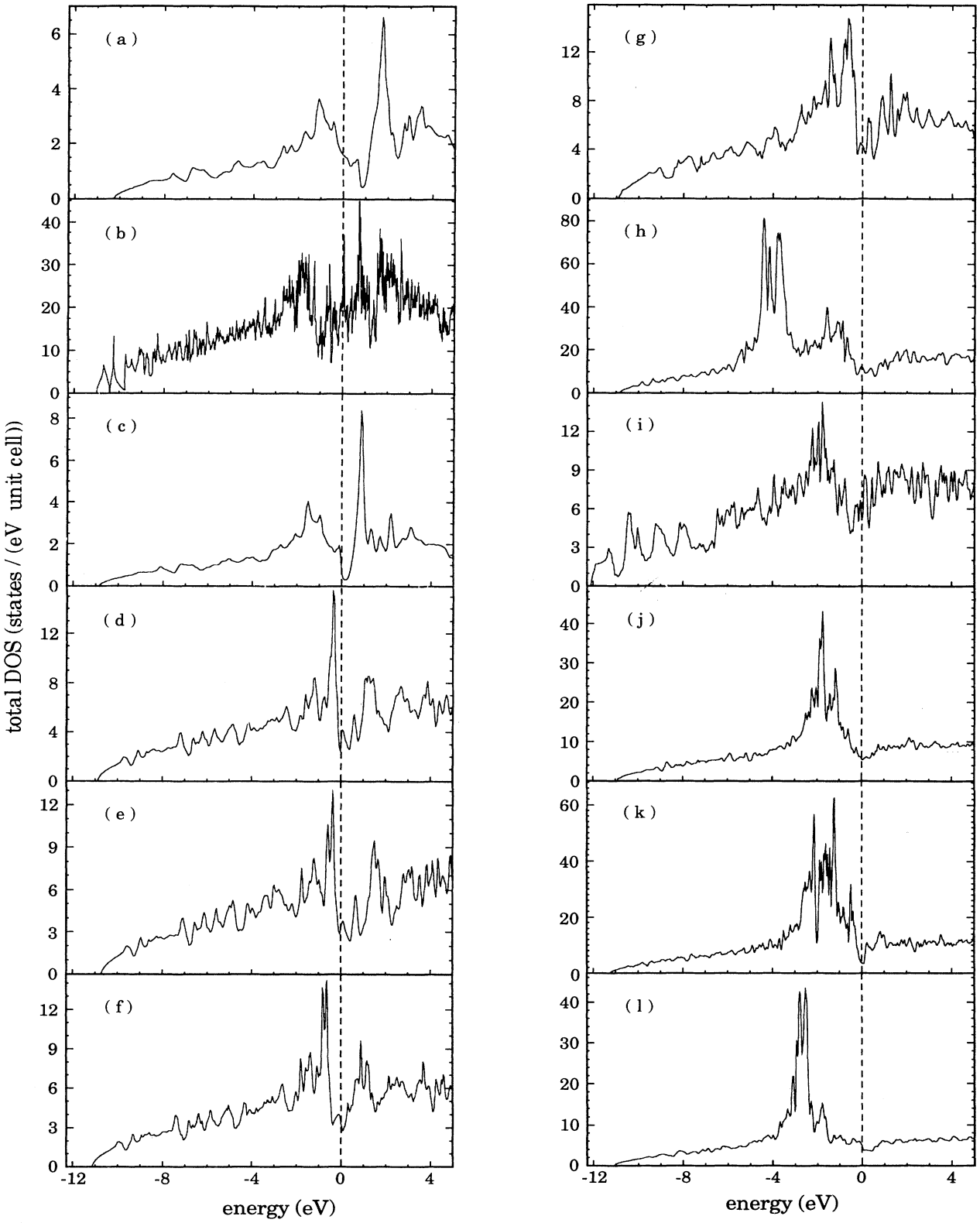

FIG. 1. Total DOS: (a) Al_3Ti, (b) $Al_{10}V$, (c) Al_3V, (d) $Al_{12}Cr$, (e) $Al_{12}Mo$, (f) $Al_{12}Mn$, (g) Al_6Mn, (h) Al_7Cu_2Fe, (i) $Al_8Mg_3Si_6Fe$, (j) Al_9Co_2, (k) Al_5Co_2, and (l) Al_3Ni. The vertical dashed lines show the Fermi level.

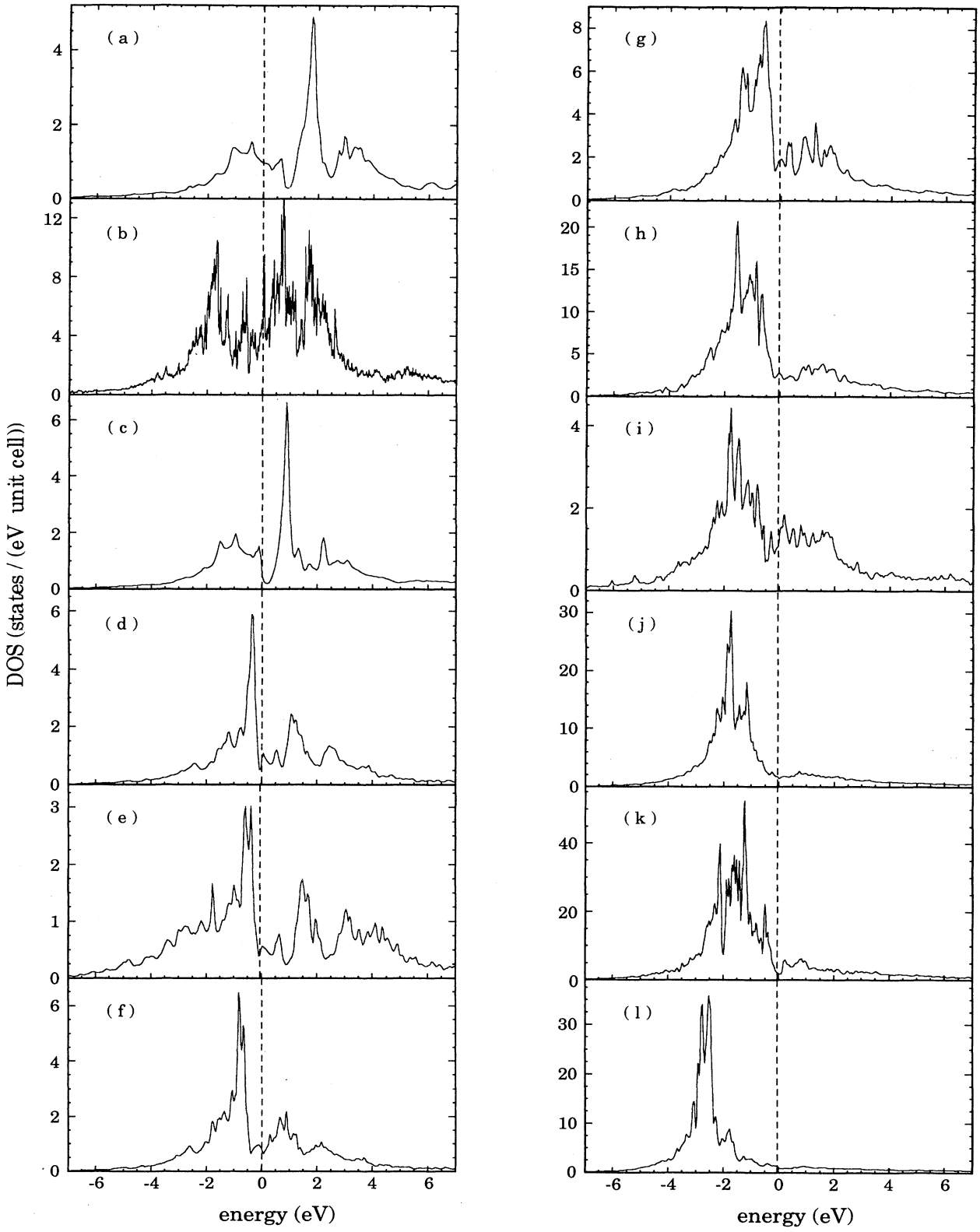

FIG. 2. Local *d* DOS on transition atoms (TM=Ti, V, Cr, Mo, Mn, Fe, Co, Ni): (a) Al_3Ti, (b) $Al_{10}V$, (c) Al_3V, (d) $Al_{12}Cr$, (e) $Al_{12}Mo$, (f) $Al_{12}Mn$, (g) Al_6Mn, (h) Al_7Cu_2Fe, (i) $Al_8Mg_3Si_6Fe$, (j) Al_9Co_2, (k) Al_5Co_2, and (l) Al_3Ni. The vertical dashed lines show the Fermi level.

DOS of Al_2Cu crystal,[53] which does not have a d peak near E_F, has no obvious pseudogap near E_F. The special effect of the transition-metal element on this pseudogap will be discussed in Sec. IV. It should be noted that the pseudogap near E_F in crystals is less deep than the pseudogap found in an approximant of icosahedral[7,8,54,55] and decagonal[36,56] quasicrystals. This is understandable since the predominant Brillouin zone of crystals is less spherical than the predominant Brillouin zone of quasicrystals and therefore the interaction between this zone and the Fermi sphere is smaller in crystals than in quasicrystals.[5] In total DOS's, there are also other valleys less pronounced than the pseudogap near E_F. Each of them should correspond to diffraction by Bragg planes associated with strong peaks in the diffraction pattern (Sec. IV A).

(iii) The local d DOS on TM atoms (Ti, V, Cr, Mo, Mn, Fe, Co, Ni), mainly due to d states, are shown in Fig. 2. The d peaks of TM are located near E_F and the pseudogap. A strong deviation from the virtual bound state Lorentzian is observed and the pseudogap near E_F is clearly seen in d DOS. The width of the d band varies with TM element from ~ 2 eV for Al_3Ni to ~ 4 eV for $Al_{10}V$ and Al_3V. This shows a strong hybridization of d orbitals and sp band. Moreover, the local d TM DOS at E_F is an important component of the total DOS (Table IV). This emphasizes the importance of transition-metal elements on the electronic structure at E_F, and thus on transport properties.

In the case of Al_7Cu_2Fe and Al_2Cu,[53] the d peak of Cu is located at about 4 eV under E_F [Fig. 1(h)] and the local DOS on Cu atoms at E_F is very small.

(iv) In studied alloys, except in $Al_{10}V$, the total DOS is rather smooth and without any fine structure. The case of $Al_{10}V$ is slightly different as its DOS is a set of fine peaks. To check that those peaks are not computational artifacts we increase the number of $\mathbf{k}$ points in the first Brillouin zone from 729 to 17 576 $\mathbf{k}$ points, without significant change in the fine structure of the DOS. The width of those peaks varies from ~ 30 to ~ 70 meV, and they should be distinguished from valleys (or pseudogaps) discussed in previous paragraphs. Their presence in $Al_{10}V$ and not in other studied alloys seems to be correlated with structural differences. Indeed, the structure of $Al_{10}V$ is characterized[45] by the presence of one compact icosahedral cluster of 12 Al atoms centered on 1 V atom. The strong Al-V interaction within this cluster plays an important role[45] in the formation of complex $Al_{10}V$ structure. Hence, we propose that the fine peaks in $Al_{10}V$ DOS may be a qualitative signature of the discrete energy levels of the cluster alone. In this scheme, fine peaks are not only due to the potential of V atoms, but they are due to the strong potential of the compact cluster composed by 12 Al and 1 V atoms. Let us note that this fine structure is comparable with the very spiky structure found by Fujiwara in an approximant of AlMnSi quasicrystal[7] and later in approximants of AlCuLi,[8] AlCuFe,[36,55], AlPdMn,[54] and AlZnMg (Ref. 54) quasicrystals.

Finally, comparisons between calculated DOS and spectroscopy measurements (soft x-ray spectroscopy and photoelectron spectroscopy) have been done elsewhere for Al_6Mn,[57] Al_7Cu_2Fe,[53] Al_5Co_2,[58] and Al_2Cu.[53] In these four alloys, good agreement is found between theoretical and experiment results.

IV. ANALYSIS OF RESULTS

To discuss electronic structures presented above, it is convenient to consider the following Anderson Hamiltonian[27] of nearly free sp electrons and d impurities located on sites i:

$$H=\sum_{i\sigma} E_{di\sigma} n_{i\sigma}+\sum_{\mathbf{k}\sigma} E_{\mathbf{k}} n_{\mathbf{k}\sigma}+\sum_{\mathbf{K}_\sigma} V_B(\mathbf{K}) c^{\dagger}_{\mathbf{k}+\mathbf{K},\sigma} c_{\mathbf{k},\sigma} + \sum_{i\mathbf{k}\sigma} V_{\mathbf{k}i}\{c^{\dagger}_{\mathbf{k}\sigma} c_{i\sigma}+c^{\dagger}_{i\sigma} c_{\mathbf{k}\sigma}\} \ . \quad (3)$$

$E_{di\sigma}$ is the self-consistent on-site d energy of the d orbital $i\sigma$ (σ spin), $E_{\mathbf{k}}$ is energy of the free-electron $\mathbf{k}\sigma$ and $n_{\mathbf{k}\sigma}, n_{i\sigma}$ are the number of electrons in $\mathbf{k}\sigma$ and $i\sigma$. V_B is the potential seen by sp electrons due to the diffraction by Bragg planes without sp-d coupling (this term was not taken into account in Ref. 27). The last term is the hopping between sp states and localized d states. We neglected the d-d interaction as there are no next-neighboring TM atoms in our studied alloys. This Hamiltonian [Eq. (3)] is written in the paramagnetic case. In the magnetic case (Sec. IV E) one has to add a Coulomb repulsive term $Un_{d\downarrow}n_{d\uparrow}$.

A. Diffraction by Bragg planes of sp states

The diffraction by Bragg planes couples the sp states to each other and leads to the formation of bonding and antibonding sp states. Schematically free sp states $|\mathbf{k}\rangle$ are diffracted by an effective pseudopotential $V_{\text{eff}}(\mathbf{K})$. $V_{\text{eff}}(\mathbf{K})$ is due both to the diffraction by Bragg planes (corresponding to the reciprocal vector $\mathbf{K}$) and to the sp-d coupling. This will be discussed in more detail in the next sections (Sec. IV B). $V_{\text{eff}}(\mathbf{K})$ couples two states $|\mathbf{k}\rangle$ and $|\mathbf{k}-\mathbf{K}\rangle$ and forms one bonding state and one antibonding state. This results in a valley in the DOS of sp electrons, located at the energy $E(\mathbf{K})$. In this simple scheme, the width of a valley associated with $\mathbf{K}$ is roughly $2V_{\text{eff}}(\mathbf{K})$.[59] To analyze these valleys in a more qualitative manner, we draw the self-consistent total sp DOS, n_{sp} (Fig. 3, full lines) in the case of Al_3Ti, Al_6Mn, Al_7Cu_2Fe, and Al_9Co_2. Here n_{sp} is the sum of the partial sp DOS of all atoms in a unit cell. Approximately, sp electrons correspond to conduction electrons because the contribution of d states to conduction states should be very low. In these figures, the valleys due to diffraction by Bragg planes are clearly observed. In principle, it should be possible to index each valley with the energy $E(\mathbf{K}_i)$ of some $\mathbf{K}_i$ vectors corresponding to intense peaks in the x-ray diffraction pattern. For instance, on the sp-DOS of Al_3Ti [Fig. 3(a)], we report the energy $E(\mathbf{K}_i)$ of the most intense peaks $\mathbf{K}_i$, as follows: $\mathbf{K}_1$, $(hkl)=(002)$; $\mathbf{K}_2$, $(hkl)=(101)$; $\mathbf{K}_3$, $(hkl)=(110)$; $\mathbf{K}_4$, $(hkl)=(112)$ and (103); $\mathbf{K}_5$, $(hkl)=(004)$; $\mathbf{K}_6$, $(hkl)=(200)$. $E(\mathbf{K}_i)$ are calculated using spectroscopy data assuming free-electron

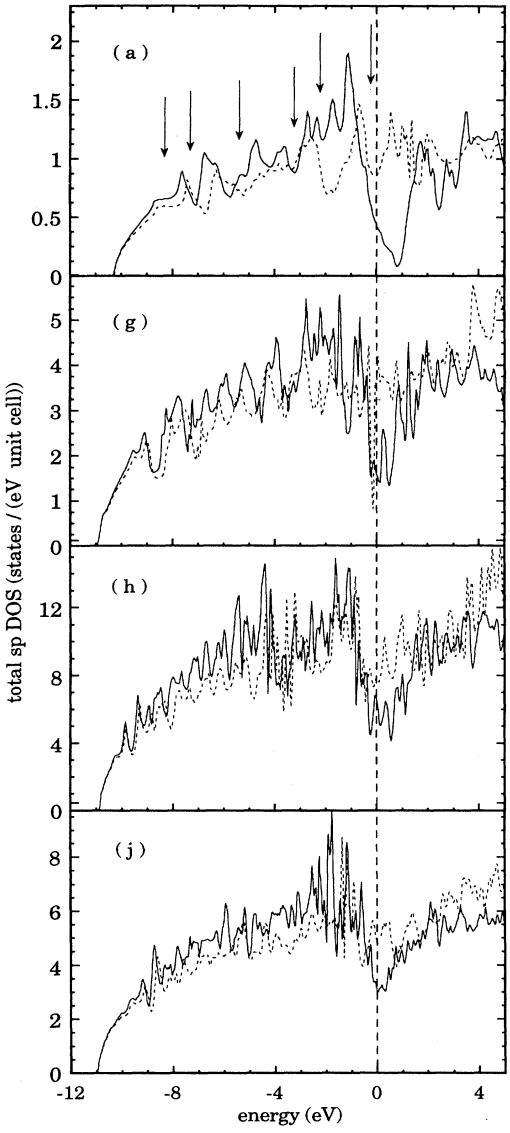

FIG. 3. Total *sp* DOS (full lines); (a) Al_3Ti [the vertical arrows show the energies $E(\mathbf{K}_i)$—see text], (g) Al_6Mn, (h) Al_7Cu_2Fe, and (j) Al_6Co_2. The *sp* DOS calculated], without *sp-d* hybridization are drawn in dotted lines. The vertical dashed lines show the Fermi level.

band. The correspondence between $E(\mathbf{K}_i)$ and some valleys is qualitatively good, which confirms the importance of diffraction by Bragg planes in this system. For Al_3V, a similar comparison can be done easily, but the other studied alloys have too many intense peaks in their diffraction pattern and this comparison is more difficult to make.

Among the different valleys on the DOS the deepest one is always located near the Fermi level. This valley, commonly called the pseudogap, corresponds to the condition given by Eq. (1). Below the minimum of the pseudogap the *sp* states are preferentially bonding *sp* states and above the minimum of the pseudogap the *sp* states are preferentially antibonding *sp* states. The band energy is minimum when bonding states are full and antibonding states are still empty, in which case the Fermi level falls in the pseudogap. This phenomenon is known to stabilize crystalline and quasicrystalline Hume-Rothery phases. The width of the pseudogap varies from 0.3 to 1 eV, which corresponds roughly to a pseudopotential $V_{\text{eff}}(\mathbf{K})$ ranging from 0.15 to 0.5 eV.[59]

B. Origin of pseudopotential

We now focus on the well-pronounced pseudogap located in the vicinity of E_F. As discussed previously it is commonly accepted that such a pseudogap is due to diffraction by Bragg planes (Hume-Rothery stabilization). On the other hand, the *sp-d* hybridization in alloys containing a small concentration of TM was studied by Friedel[26] and Anderson.[27] Their model leads to a Lorentzian *d* band, but it does not take into account the diffraction by Bragg planes of *sp* electrons. Here, we would like to analyze the effect of *sp-d* hybridization on the formation the pseudogap near E_F, in the presence of diffraction by Bragg planes.

By suppressing the corresponding matrix structure factor $S_{RLR'L'}$ in the LMTO Hamiltonian, we can calculate the DOS without *sp-d* hybridization (see Sec. II). Starting from self-consistent potential parameters calculated with the real Hamiltonian, we calculate the eigenstate of the Hamiltonian without *sp-d* coupling and the corresponding *sp* DOS without *sp-d* hybridization named n'_{sp} (dashed lines on Fig. 3). Comparison between n_{sp} and n'_{sp} leads to the following remarks.

The difference between the pseudopotential in n_{sp} and n'_{sp} depends on the alloys. Nevertheless, a lot of valleys present in n_{sp} are less pronounced in n'_{sp}. This suggests that the *sp-d* hybridization increases the valleys created by the diffraction by Bragg planes. Moreover, the difference between the pseudogap near E_F in n_{sp} and n'_{sp} is more pronounced. In some alloys, such as Al_3Ti, Al_3V, and $Al_{12}Mn$, *sp-d* hybridization strongly increases the depth and the width of the pseudogap. On some of the other alloys such as Al_7Cu_2Fe this effect is present but less pronounced. In a third group of alloys, such as Al_3Ni, the pseudogap is not present in n'_{sp}. These last results have also been found in Al_2Ru and Ga_2Ru semiconductor alloys,[31] where the *sp-d* hybridization seems to create the gap.

These results suggest that one might consider an effective pseudopotential V_{eff}, which is the origin of the pseudogap at the E_F, as follows:

$$V_{\text{eff}} = V_B + \frac{|V_d|^2}{E - E_d} \ . \tag{4}$$

Here, V_d is an operator that couples two *sp* states $|\mathbf{k}\rangle$ and $|\mathbf{k}-\mathbf{K}_d\rangle$ via the *sp-d* coupling [last term of the Hamiltonian, Eq. (3)], and K_d a vector of the reciprocal lattice of the TM atom network. In the studied alloys, the reciprocal lattice of the TM atom network is almost the same with the reciprocal lattice of the alloy.

The V_B term does not depend on the *sp* electron energy E and corresponds to the usual diffraction of nearly free

electrons by the Bragg planes of the predominant Jones zone. The term V_d gives the effect of the scattering by d states of sp states. This last term of the pseudopotential depends on energy and is important in the vicinity of the d energy E_d. In Hume-Rothery alloys containing transition-metal elements, the combined effect of these two terms, corresponding to the diffraction by Bragg planes of sp states and the scattering of sp states by d states (via sp-d coupling), respectively, is essential in the formation and the importance of the pseudogap at the Fermi level.

C. Apparent negative valence of transition-metal atom

Effects of sp-d hybridization may give a possible explanation for the apparent negative valence of TM atoms in Hume-Rothery alloys proposed by Raynor.

The valences of the Al and Cu atoms are known (3 electrons per atom, and between 1 and 1.5 electrons per atom, respectively). But the valence of TM is undetermined because of the unfilled d band. Raynor proposed to calculate the valence of TM as follows. From the diffraction measurements the predominant Brillouin zone of an alloy can be determined. Considering a free-electron band, he calculated the valence of TM in such a way that the Hume-Rothery condition of stabilization is satisfied, i.e., under the requirement that the Fermi sphere should touch the predominant Brillouin zone [Eq. (1)]. In this fashion, the calculated valence of the TM in Al-TM and Al-Cu-TM compounds is always found to be negative. In this scheme, the apparent negative valence corresponds to an amount of sp electrons (conduction electrons) N_{e-} transferred on d orbitals of the TM. Such an apparent negative valence, or charge transfer, is generally found between -1 and -3 electrons per TM atom.[18,24] Nevertheless, Wenger and Steineman[25] estimated, by analyzing the soft x-ray line intensities, that charge transfer on the TM atom is lower than 0.5 electron per TM atom in $Al_{1-x}TM_x$ alloys ($x<0.3$). Moreover, *ab initio* calculations confirm the small charge transfer on TM (see Refs. 7, 8, 41, 55, and 56 and Sec. II above). This small charge transfer of TM atoms is not sufficient to explain the negative valence of TM.

The strong effect of sp-d hybridization on sp band suggests a new explanation for the apparent negative valence. Indeed, we can calculate the number of sp electrons (conduction electrons) associated to the effects of sp-d hybridization, N_{e-}, as follows:

$$N_{e-}=\int_{-\infty}^{E_F}(n_{sp}-n'_{sp})dE \ . \tag{5}$$

In all the studied alloys N_{e-} is positive and gives an increase of sp electrons due to the presence of transition-metal elements. Then assuming a small charge transfer from sp band to d orbitals of TM atoms ($-N_{e-}$) can be viewed as an apparent negative valence of TM. The values of ($-N_{e-}$), calculated from LMTO results,[33,34] are in good agreement with the experimental apparent negative valence.

Friedel[28] has proposed an alternative explanation for the apparent negative valence of TM in an sp matrix. He argues that, in the presence of TM, stabilization is not obtained when Eq. (1) is satisfied but when $2k_F>K_i$ such that the Fermi surface enclosed the predominant Brillouin zone. In that scheme, the apparent negative valence of TM comes from underestimation of total electron valence calculated by Eq. (1). This explanation is not really in contradiction with ours and both phenomena could contribute to the apparent negative valence. However, it is qualitatively and quantitatively clear from Eq. (5) that the apparent negative valence of the TM atom in our model is directly related to the sp-d hybridization effects in the electronic structure of these alloys.

D. sp-d hybridization: role of TM atom position

In the previous section we have shown that the sp-d hybridization gives a great contribution to the DOS. We now want to study how d states are coupled with the sp states in the presence of pseudopotential $V_B(\mathbf{K})$.

In the studied alloys, TM atoms are in low concentration and it is interesting to analyze the sp-d coupling in terms of the one-electron Green's function in the subspace of the d orbitals G_d. Considering ten degenerated d states per TM atom and neglecting the d-d hybridization, G_d can be directly calculated from the d partial density of states $n_d(E)$. The basic quantity is the self-energy, $\sigma(z)$:

$$\begin{aligned} n_d(E)&=-\frac{1}{\pi}\lim_{\varepsilon\to 0^+}G_d(E+i\varepsilon) \ , \\ G_d(z)&=\frac{1}{z-E_d-\sigma_d(z)} \end{aligned} \tag{6}$$

by definition, $\sigma(z)$ represents the energy of the sp-d coupling:

$$\mathrm{Im}[\sigma(E+i\varepsilon)]=-\pi N(E)\overline{V^2}(E) \ . \tag{7}$$

$\overline{V^2}(E)$ is the mean coupling strength between the d orbital and the eigenstates $|\alpha\rangle$ of sp states. $N(E)$ is the average density of sp states. In the absence of diffraction by Bragg planes (virtual bound state), $N(E)$ and $\overline{V^2}(E)$ vary on the scale of the width of the sp band. Then, $\mathrm{Im}[\sigma(E)]$ is almost constant. But when the diffraction by Bragg planes is important, $N(E)\overline{V^2}(E)$ varies strongly on the scale of the pseudopotential, $V_B(\mathbf{K})$. Assuming typical values for $V_B(\mathbf{K})$, $V_B(\mathbf{K})=0.2$ or 0.5 eV,[5] the deviation of the self-energy in the presence of diffraction by Bragg planes compared to the virtual bound state case can be important.

The self-energies calculated by Eq. (6) from LMTO d partial DOS are reported on Fig. 4. For Al_3Ti, Al_3V, and $Al_{10}V$ the quantity $-\mathrm{Im}[\sigma(z)]$ is stronger for the energy under the pseudogap. This suggests that d states are more strongly coupled with bonding states, which are under the minimum of the pseudogap. In all other cases, the peak of $-\mathrm{Im}[\sigma(z)]$ appeared below the pseudogap and the d states are preferentially coupled with antibonding states.

The present results are in qualitatively good agreement with a simple model that we have developed elsewhere[33,34] in the impurity limit for transition-metal atoms. In this model, we consider nearly free sp states

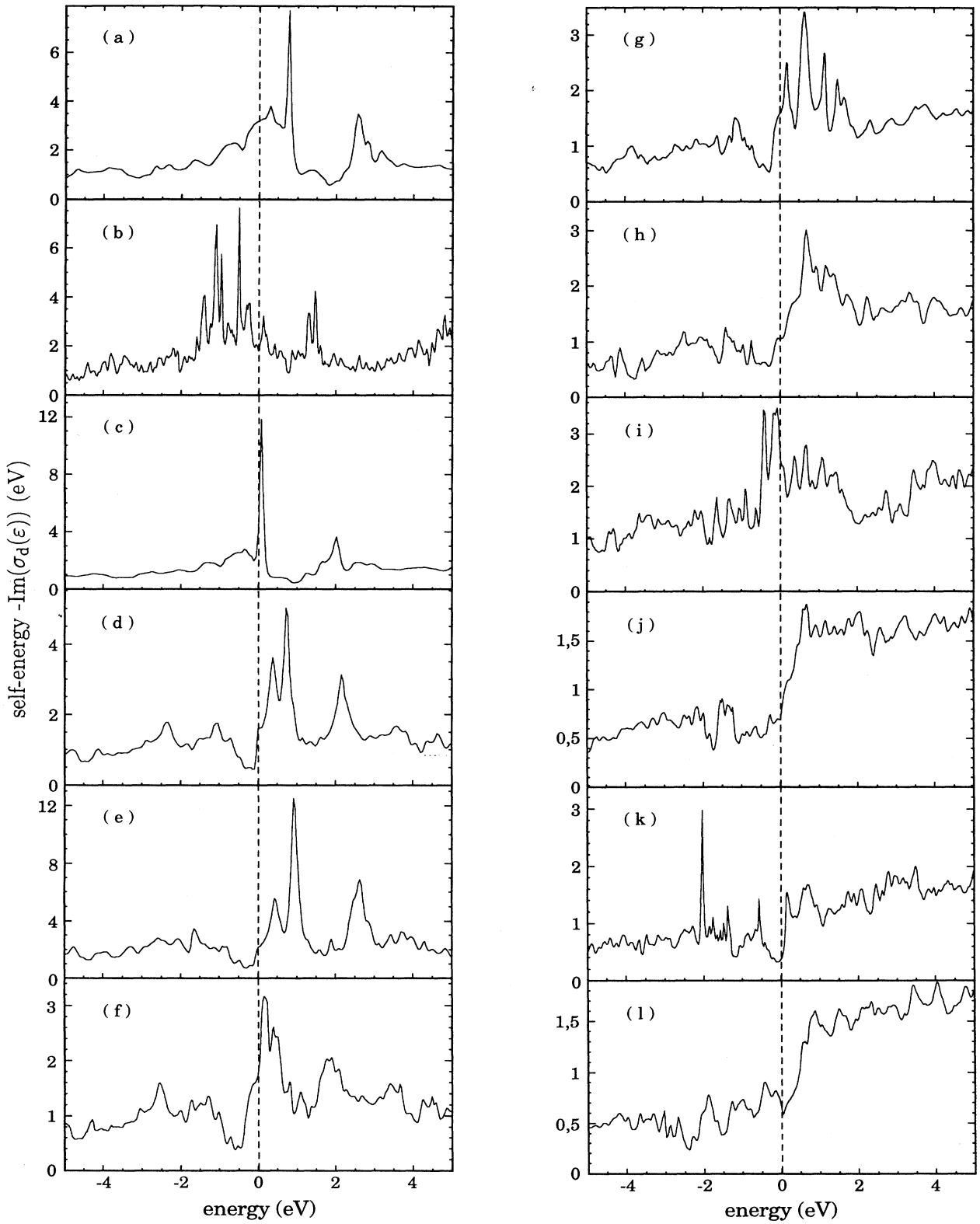

FIG. 4. Self-energy ($-\mathrm{Im}[\sigma_d(z)]$): (a) Al_3Ti, (b) $Al_{10}V$, (c) Al_3V, (d) $Al_{12}Cr$, (e) $Al_{12}Mo$, (f) $Al_{12}Mn$, (g) Al_6Mn, (h) Al_7Cu_2Fe, (i) $Al_8Mg_3Si_6Fe$, (j) Al_9Co_2, (k) Al_5Co_2, and (l) Al_3Ni. The vertical dashed lines show the Fermi level.

(with diffraction by Bragg planes) coupled with ten degenerate d states per impurity. The number of d electrons is a parameter of the model and varies to simulate all TM from Ti to Ni. The main result of this model is a well-pronounced pseudogap in the d DOS, and an increase of the sp DOS, due to the sp-d hybridization. Moreover, an important result of this model is that d orbitals are preferentially coupled with bonding or antibonding sp states depending on the position of the transition-metal atom in the unit cell. According to the number of d electrons in the d band, two cases appear:[34] For Ti and V impurity, the Fermi level is located in the pseudogap (d peak) when the d orbital is preferentially coupled with bonding (antibonding) sp states. The energetically favorable case is when E_F lies in the pseudogap, in which case V and Ti d orbitals should be preferentially coupled with bonding sp states as we found in real alloys. For other TM impurities (Cr, Mn, Fe, Co, and Ni), the energetically favorable case is when the d orbital is preferentially coupled with antibonding sp states as found in real studied alloys (previous paragraph).

The good agreement between real calculations of electronic structures in crystals and a simple model simulating the combined effects of the diffraction by Bragg planes and the sp-d hybridization suggests that this effect is crucial to the understanding of the electronic structure and the stability of Hume-Rothery alloys containing TM.

It is also important to mention the possible existence of d nonbonding peaks. Those peaks correspond to d states not coupled (or weakly coupled) with sp states and depend on the local symmetry around the TM atoms and the one-site d energy level, E_d. The existence of nonbonding states has been shown by *ab initio* calculations in comparison to several atomic structures with the same composition in the cases of Al_3Ti (Ref. 41) and $Al_{13}Ru_4$.[60] It seems[60] that such a nonbonding peak may disappear in less symmetric alloys (crystals, 2D quasicrystals), but is always present in highly symmetric ones. In the present work, we do not compare different structures with the same composition and we cannot conclude on the presence or not of the d nonbonding peaks. Nevertheless, some peaks in the d DOS (Fig. 2), located at an energy E where sp-d coupling is small—i.e., when $-\mathrm{Im}[\sigma(E)]$ is small (Fig. 4)—may be nonbonding peaks.

E. Magnetism of Hume-Rothery alloys with TM

The presence of the pseudogap at the Fermi level may have a strong influence on magnetic properties, especially on the criterion for the appearance of magnetic moments and spin susceptibility in paramagnetic cases.

In the Hartree-Fock approximation considering the limit case of the virtual bound state, the criterion for the appearance of a magnetic moment is[27,61] $Un_d(E_F)>1$, where U is the one-site Coulomb repulsion energy between two d electrons and $n_d(E_F)$ the d DOS of d impurity at E_F. Due to the combined effect of diffraction by Bragg planes and sp-d hybridization, this criterion should be changed into

$$U\left|\frac{dN_d}{dE_d}\right|>1\ , \tag{8}$$

where N_d is the number of electrons on the d orbital and E_d the d energy level. Without any diffraction by Bragg planes this new criterion is equivalent to the criterion $Un_d(E_F)>1$. But in Hume-Rothery alloys characterized by a strong diffraction associated with a pseudogap at E_F, this criterion shows that the appearance of magnetic moments is not directly related to $n_d(E_F)$.

The magnetic spin susceptibility χ can also be calculated using

$$\chi=\chi_d+\chi_{sp}\ , \tag{9}$$

where χ_d is the contribution from the d band and χ_{sp} is that from the sp band. These two contributions can be split as follows:

$$\begin{aligned}&\chi_d=\chi_{0d}+\Delta\chi_d \quad \text{with} \quad \chi_{0d}=\mu^2 n_d(E_F)\ ,\\ &\chi_{sp}=\chi_{0sp}+\Delta\chi_{sp} \quad \text{with} \quad \chi_{0sp}=\mu^2 n_{sp}(E_F)\ ,\end{aligned} \tag{10}$$

where μ is the Bohn magneton, χ_{0d} and χ_{0sp} are the normal Pauli paramagnetic contributions for noninteracting electrons, and $\Delta\chi_d$ and $\Delta\chi_{sp}$ are the contributions due to interaction between electrons. Within the Hartree-Fock approximation, one can easily calculate the susceptibility contribution due to the d-d electron interaction on the same atomic site (sp-sp electron interactions and sp-d electron interactions are neglected):

$$\begin{aligned}&\Delta\chi_d=a\alpha \quad \text{and} \quad \Delta\chi_{sp}=a[n_d(E_F)-\alpha]\ ,\\ &\alpha=-\frac{dN_d}{d\varepsilon_d}>0\ (N=N_\sigma) \quad \text{and} \quad a=2\mu U\frac{n_d(E_F)}{1-U\alpha}\ .\end{aligned} \tag{11}$$

In the virtual bound states case $\alpha=n_d(E_F)$ and $\Delta\chi_{sp}\approx 0$ (compensation theorem[26,27]). But considering diffraction by Bragg planes, $\Delta\chi_{sp}$ may become negative even though $\Delta\chi_d$ is always positive. This has been shown in the limit of d impurity coupled with sp states diffracted by the Bragg plane of a predominant Brillouin zone.[62] In the limit case close to magnetic transition (i.e., $1-U|\alpha|\approx 0$), when $\Delta\chi_{sp}$ is negative, we could expect to have $\chi_d>0$ and $\chi_{sp}<0$. This corresponds to the paramagnetic moment on the d electrons of TM and the diamagnetic moment on the sp electrons surrounding the TM atoms.

In alloys characterized by a strong diffraction by some Bragg plane (Hume-Rothery alloys, quasicrystals, etc.) containing TM, this could have consequences on experiments that are sensitive to the susceptibility of sp states such as NMR experiments. Indeed, it is found that some quasicrystalline systems have a local sp susceptibility surrounding the TM atoms, which is abnormally small or even negative.[63] This preliminary study of magnetism in Hume-Rothery alloys deserves further investigations.

V. CONCLUSION

We have performed a scalar relativistic self-consistent electronic structure calculation for Hume-Rothery alloys

with a matrix of aluminum and containing transition-metal atoms in small concentration. The LMTO calculations predict the existence of a quite pronounced pseudogap at or near the Fermi level. This pseudogap exists in both *sp* and *d* bands and is more pronounced for alloys containing TM atoms of the middle of the *d* series, i.e., when the one-site *d* energy level is near the Fermi level. It is well known that this pseudogap is due to the diffraction by Bragg planes. Nevertheless, our calculations suggest that the presence of *d* states increases the pseudogap via the *sp-d* hybridization. In the Al_2Ru and Ga_2Ru semiconductor crystals, this effect is essential in the formation of the gap. Moreover, the role of the TM atomic position in the structure on the pseudogap formation and the local electronic stability has been emphasized. As a consequence, this suggests the crucial influence of the TM atomic positions (and TM concentration) on transport properties. To conclude, it seems that the well-pronounced pseudogap at E_F results from a combined effect of the strong interaction between the Fermi surface and a predominant Brillouin zone, and the *sp-d* hybridization.

Another interesting result is the fine peaks in the DOS of $Al_{10}V$, which reminds us of the very spiky DOS found in large approximants of quasicrystals. This spiky structure may be the signature of the presence of atomic clusters in these alloys and it requires further investigations.[64]

ACKNOWLEDGMENTS

The authors are grateful to J. Friedel, T. Fujiwara, N. W. Ashcroft, E. Belin, C. Berger, and T. Klein for stimulating and fruitful discussions. D.N.M. thanks the University Joseph Fourier and CNRS for financial support.

*Present address: Department of Materials, University of Oxford, Oxford, Parks Road, OX1 3PH, United Kingdom.

[1]W. Hume-Rothery, J. Inst. Met. **35**, 295 (1926); W. Hume-Rothery and G. V. Raynor, *The Structure of Metals and Alloys* (Institute of Metals, London, 1954).
[2]H. Jones, Proc. Phys. Soc. **49**, 250 (1937).
[3]T. B. Massalski and U. Mizutani, Prog. Mater. Sci. **22**, 151 (1978).
[4]J. Friedel and F. Denoyer, C. R. Acad. Sci. Paris Ser. II **305**, 171 (1987).
[5]A. P. Smith and N. W. Ashcroft, Phys. Rev. Lett. **59**, 1365 (1987).
[6]V. G. Vaks, V. V. Kamyshenko, and G. D. Samolyuk, Phys. Lett. A **132**, 131 (1988).
[7]T. Fujiwara, Phys. Rev. B **40**, 942 (1989).
[8]T. Fujiwara and T. Yokokawa, Phys. Rev. Lett. **66**, 333 (1991).
[9]T. Klein, C. Berger, D. Mayou, and F. Cyrot-Lackmann, Phys. Rev. Lett. **66**, 2907 (1991); J. L. Wanger, B. D. Biggs, and S. J. Poon, *ibid.* **65**, 203 (1990).
[10]E. Belin and A. Traverse, J. Phys. Condens. Matter **3**, 2157 (1991); M. Mori, S. Matsuo, T. Ishimasa, T. Matsuura, K. Kamiya, H. Inokuchi, and T. Matsukawa, *ibid.* **3**, 767 (1991).
[11]J. B. Dunlop, G. Grüner, and A. D. Caplin, J. Phys. F **4**, 2203 (1974).
[12]S. J. Poon, Adv. Phys. **41**, 303 (1992); C. Berger, in *Lecture on Quasicrystals,* edited by F. Hippert and D. Gratias (Les Editions de Physique, Les Ulis, France, 1994), p. 463.
[13]D. Mayou, *Lecture on Quasicrystals* (Ref. 12), p. 417.
[14]A. D. I. Nicol, Acta Crystallogr. **6**, 285 (1953).
[15]M. G. Bown and P. J. Brown, Acta Crystallogr. **9**, 911 (1956).
[16]G. V. Raynor and M. B. Waldron, Philos. Mag. **40**, 198 (1949).
[17]A. M. B. Douglas, Acta Crystallogr. **3**, 19 (1950).
[18]P. A. Bancel and P. A. Heiney, Phys. Rev. B **33**, 7917 (1986).
[19]B. D. Biggs, S. J. Poon, and N. D. Munirathnam, Phys. Rev. Lett. **65**, 2700 (1990).
[20]P. Lanco, T. Klein, C. Berger, F. Cyrot-Lackmann, G. Fourcaudot, and A. Sulpice, Europhys. Lett. **18**, 227 (1992).
[21]H. Akiyama, Y. Honda, T. Hashimoto, K. Edagawa, and S. Takeuchi, Jpn. J. Appl. Phys. **32**, L1003 (1993); F. S. Pierce, S. J. Poon, and Q. Guo, Science **261**, 737 (1993); C. Berger, T. Grenet, P. Lindqvist, P. Lanco, J. C. Grieco, G. Fourcaudot, and F. Cyrot-Lackmann, Solid State Commun. **87**, 977 (1993).
[22]F. S. Pierce, P. A. Bancel, B. D. Biggs, Q. Guo, and S. J. Poon, Phys. Rev. B **47**, 5670 (1993).
[23]P. Lindqvist, C. Berger, T. Klein, P. Lanco, and F. Cyrot-Lackmann, Phys. Rev. B **48**, 630 (1993).
[24]G. V. Raynor, Prog. Met. Phys. **1**, 1 (1949).
[25]A. Wenger and S. Steinemann, Helv. Phys. Acta **47**, 321 (1974).
[26]J. Friedel, Can. J. Phys. **34**, 1190 (1956).
[27]P. W. Anderson, Phys. Rev. **124**, 41 (1961).
[28]J. Friedel, Helv. Phys. Acta **61**, 538 (1988).
[29]J. Deutz, P. H. Dederichs, and R. Zeller, J. Phys. F **11**, 1787 (1981).
[30]P. P. Singh, J. Phys. Condens. Matter **3**, 3285 (1991).
[31]D. Nguyen Manh, G. Trambly de Laissardière, J. P. Julien, D. Mayou, and F. Cyrot-Lackmann, Solid State Commun. **82**, 329 (1992).
[32]F. S. Pierce, S. J. Poon, and B. D. Briggs, Phys. Rev. Lett. **70**, 3919 (1993).
[33]G. Trambly de Laissardière, D. Mayou, and D. Nguyen Manh, Europhys. Lett. **21**, 25 (1993); D. Mayou, F. Cyrot-Lackmann, G. Trambly de Laissardière, and T. Klein, J. Non-Cryst. Solids **153&154**, 412 (1993).
[34]G. Trambly de Laissardière, D. Nguyen Manh, and D. Mayou, J. Non-Cryst. Solids **153&154**, 430 (1993).
[35]J. Friedel, Philos. Mag. B **65**, 1125 (1992).
[36]T. Fujiwara and H. Tsunetsugu, in *Quasicrystals: The States of the Art,* edited by D. P. Di Vincenzo and P. J. Steinhart (World Scientific, Singapore, 1991), p. 343.
[37]J. Zou and A. E. Carlsson, Phys. Rev. Lett. **70**, 3748 (1993).
[38]L. Do Phoung, D. Nguyen Manh, and A. Pasturel, Phys. Rev. Lett. **71**, 372 (1993).
[39]P. Villars and L. D. Calvet, *Pearson's Handbook of Crystallographie Data for Intermetallic Phase,* 2nd ed. (American Society for Metals, Materials Park, OH, 1991), Vol. 1.
[40]W. P. Pearson, *Handbook of Lattice Spacing and Structure of Metals* (Pergamon, New York, 1967), Vol. 2.
[41]A. E. Carlsson, Phys. Rev. B **43**, 12 176 (1991).

[42]T. Hong and A. J. Freeman, J. Mater. Res. **6**, 330 (1991); J.-H. Xu and A. J. Freeman, *ibid.* **6**, 1188 (1991); A. T. Paxton and D. G. Pettifor, Scr. Metall. **26**, 529 (1992).

[43]O. K. Andersen, Phys. Rev. B **12**, 3060 (1975); O. K. Andersen, O. Jepsen, and D. Glötzel, in *Highlights of Condensed-Matter Theory,* edited by F. Bassani, F. Fumi, and M. P. Tosi (North-Holland, New York, 1985).

[44]H. L. Skriver, *The LMTO Method* (Springer-Verlag, Berlin, 1984).

[45]P. J. Brown, Acta Crystallogr. **10**, 133 (1957).

[46]P. Hohenberg and W. Kohn, Phys. Rev. **136**, B964 (1964); W. Kohn and L. J. Sham, *ibid.* **140**, A1133 (1965).

[47]O. Jepsen and O. K. Andersen, Solid State Commun. **9**, 1763 (1971).

[48]D. Guenzburger and D. E. Ellis, Phys. Rev. Lett. **67**, 3832 (1991).

[49]C. J. Smithells, *Metals Reference Handbook,* 5th ed. (Butterworths, London, 1976), p. 975.

[50]M. Nakamura and K. Kimura, J. Mater. Science **26**, 2208 (1991).

[51]*Cohesion in Metals,* edited by F. R. de Boer and D. G. Pettifor (North-Holland, Amsterdam, 1988), Vol. 1, pp. 130, 153, 202, 273, 309, and 416.

[52]U. Koster *et al.*, J. Non-Cryst. Solids **153&154**, 446 (1993).

[53]G. Trambly de Laissardière, Z. Dankházi, E. Belin, A. Sadoc, D. Nguyen Manh, D. Mayou, M. A. Keegan, and D. Papaconstantopoulos, Phys. Rev. B **51**, 14 035 (1995).

[54]J. Hafner and M. Krajčí, Europhys. Lett. **17**, 145 (1992); Phys. Rev. Lett. **68**, 2321 (1992); M. Krajčí, M. Windisch, J. Hafner, G. Kresse, and M. Mihalkovič, Phys. Rev. B **51**, 17 355 (1995).

[55]G. Trambly de Laissardière and T. Fujiwara, Phys. Rev. B **50**, 5999 (1994).

[56]G. Trambly de Laissardière and T. Fujiwara, Phys. Rev. B **50**, 9843 (1994).

[57]Z. Dankházi, G. Trambly de Laissardière, D. Nguyen Manh, E. Belin, and D. Mayou, J. Phys. Condens. Matter **5**, 3339 (1993).

[58]P. Pêcheur, E. Belin, G. Toussaint, G. Trambly de Laissardière, D. Mayou, Z. Dankházi, H. Müller, and H. Kirchmayr (unpublished).

[59]S. E. Burkov, T. Timusk, and N. W. Ashcroft, J. Phys. Condens. Matter **4**, 9447 (1992).

[60]D. Nguyen Manh, A. T. Paxton, D. G. Pettifor, and A. Pasturel, Intermetallics **3**, 9 (1995).

[61]A. Blandin and J. Friedel, J. Phys. Radium **20**, 160 (1959).

[62]D. Mayou, G. Trambly de Laissardière, and F. Cyrot-Lackmann, in *Proceedings of the International Conference on the Physics of Transition Metals, Darmstadt, 1992,* edited by D. M. Oppeneer and J. Kübler (World Scientific, Singapore, 1993), p. 318.

[63]F. Hippert (private communication).

[64]G. Trambly de Laissardière, S. Roche, and D. Mayou (unpublished).